Hydrogen-terminated diamond electrodes. II. Redox activity

Wenying Zhang, Jürgen Ristein, and Lothar Ley
Technical Physics, University of Erlangen, Germany
(Received 18 April 2008; revised manuscript received 18 June 2008; published 9 October 2008)

One of the most attractive features of diamond is its robust *p*-type surface conductivity that develops spontaneously under atmospheric conditions on hydrogen-terminated samples. An electrochemical charge transfer between diamond and an air-borne redox couple has been suggested to be responsible for the spontaneous appearance of surface-near holes. We present direct proof for the redox activity of the diamond surface by measuring *p*H-dependent open circuit potentials and quasistatic polarization curves for hydrogen-terminated and partially oxidized diamond electrodes. Under open circuit conditions we find in fact a mixed (or corrosion) potential that is consistent with the simultaneous equilibriation of the electrode versus both the hydrogen-hydronium and the oxygen-hydroxyl redox couple. Our data show extremely long-time constants for establishing the redox equilibrium and very low exchange current densities making the identification and characterization of the redox process a demanding experimental task.

DOI: 10.1103/PhysRevE.78.041603 PACS number(s): 68.08.−p, 73.40.Mr, 73.20.−r, 72.90.+y

INTRODUCTION

In 2001, Maier *et al.* [1] suggested an electrochemical surface transfer doping model for the surface conductivity of intrinsic, hydrogen-terminated diamond, elaborating on earlier qualitative arguments by Ri *et al.* [2]. The basic mechanism in this model is the charge equilibration of the diamond surface with an electrochemical redox couple in a moisture layer under atmospheric conditions. Maier *et al.* suggested the hydrogen-hydronium redox couple $H_2+2H_2O \rightleftarrows 2H_3O^+ + 2e^-$ as a plausible candidate due to the CO_2 induced slight acidity of water under atmospheric conditions. Many experiments have since then confirmed the relevance of humidity and the beneficial effect of acidity for the diamond surface conductivity [3–5]. Recently, Chakrapani *et al.* have studied the electrochemical charge transfer of hydrogenated diamond from a different perspective. Instead of measuring the effect of redox equilibration on the diamond surface conductivity they investigated the change in *p*H and oxygen concentration in the liquid electrolyte as a consequence of the redox activity of the diamond surface. They were able to measure this normally minute effect by using diamond powder and thus enhancing the active diamond area by orders of magnitude, albeit at the expense of less-defined surface properties [6]. Their experiments confirmed the electrochemical surface transfer doping model of Maier *et al.*, suggesting, however, the oxygen-hydroxyl redox couple $O_2+2H_2O+4e^- \rightleftarrows 4OH^-$ to be the active one at the hydrogen-terminated diamond surface. Here we address the role of the two different redox couples for the surface charge and the ensuing surface conductivity of diamond in the light of new experimental results. As has been pointed out before [7] and reemphasized by Chakrapani *et al.* [6], transfer doping as we discuss it here is expected to be relevant for the electrochemical activity of other semiconducting materials as well.

The near-surface *p*-type conductivity of intrinsic hydrogenated-terminated diamond can be effectively controlled by a field effect. This has been demonstrated in purely solid-state devices [8–10] and also in combination with an electrolytic gate contact [11]. In the latter geometry of a so-called solution gate field effect transistor (SGFET), the hole density at the surface of the diamond electrode exhibits a pronounced ion sensitivity that qualifies such a device as a chemical sensor. Despite intensive research, a number of fundamental questions on this issue remained rather unclear. Particularly, the ion sensitivity with respect to protons, i.e., its *p*H response, has been discussed controversially over the years and researchers have inferred supporting [12] as well as contradicting [13] arguments with respect to the electrochemical surface transfer doping model from such experiments. Such reasoning is, however, based on a misconception because ion sensitivity and redox activity are not always carefully distinguished. Only recently, this crucial issue for the understanding of the electrochemical characteristics of the diamond surface has been clarified [14,15]. When considering the surface charge (and thus the hole density) and the surface potential, the diamond electrode in an SGFET configuration can be well described in the limit of a perfectly polarizable electrode, i.e., one that allows no charge exchange across the elecrtrode-electrolyte interface. Charge density and potential in the whole electrochemical circuit can be completely derived by considering the chemical equilibrium of ionic species in the electrolytic sections and of the electronic charge (electrons and holes) in the solid-state sections [15]. This explicitly excludes the charge transfer between diamond electrode and electrolyte. Thus, the investigation of the output and of the transfer characteristics of an SGFET yields no information about the redox activity of the electrode [15]. This important fact has not been properly appreciated by the community so far. Even in the latest presentation where the authors claim to resolve the controversy about the *p*H sensitivity of the hydrogen-terminated diamond electrode [14], it is summarized that "the *p*H sensitivity of the H-terminated diamond surface conductivity does not follow the prediction of the transfer doping model." There is no such prediction, and the ion sensitivity of the electrode yields no arguments with respect to the transfer doping model, neither pro, nor con.

Although outside the scope of the polarizable electrode approximation, there is charge transfer across the diamond-

electrolyte interface. In an SGFET architecture it is witnessed by the weak gate current (typically smaller than 10^{-9} A) that is usually ignored in experiments on transistors. It is the charge exchange across the diamond-electrolyte interface and its dependence on electrolytic composition and externally applied voltage that is in the focus of this paper. A consequence of this charge exchange is the open circuit voltage (OCV) of the diamond electrode in an electrolytic cell vs a well-defined reference electrode. We have measured the OCV as a function of the *p*H of the electrolyte for a hydrogen-terminated and a partially oxidized diamond electrode. The open circuit voltage is the voltage of zero current in the static polarization curve, and more general information is obtained from measuring this curve over a limited voltage range around the OCV. Since the time constants required to establish the open circuit voltage are extremely long, we have measured the polarization curves for *p*H7 only. For comparison, both OCV vs *p*H and polarization curves for *p*H7 have also been measured for a Pt wire electrode.

EXPERIMENT

The diamond sample used for the experiments was a type IIa intrinsic single crystal diamond plate of 5 mm by 8 mm size with a (100) surface that was hydrogen-terminated under standard conditions in a microwave driven hydrogen plasma (see [16] for details). Complete hydrogen termination was confirmed by measuring the surface conductivity under atmospheric conditions. The backside of the sample was subsequently plasma oxidized to remove the surface conductive layer. Silver paste and gold wire were used to provide a perfectly ohmic contact to the hydrogen-terminated diamond side.

Care was taken that only the diamond surface and not the metal contact was exposed to the electrolyte. This was achieved in the same way as in our experiments in the SGFET geometry without any epoxy or sealant, simply by dipping only the hydrogen-terminated diamond into the electrolyte and keeping the metal contacts out in air (see [15]). The active diamond electrode area exposed to the electrolyte was 5 mm by 3 mm. The electrolyte consisted of 10 mM phosphate buffer and 10 mM KCl which was titrated with H_3PO_4 and KOH to adjust the *p*H. The reference electrode was an electrochemical Ag/AgCl electrode (3 M KCl solution). We have chosen a double junction version to minimize contamination of the electrolyte (Schott B2220). The redox potential of that electrode is +0.20 V vs standard hydrogen electrode (SHE) at room temperature.

The complete electrical circuit is sketched in Fig. 1. The characteristic marks along the path from x_1 to x_8 will be referred to when discussing the experimental results. In the following all voltages will be specified with respect to the reference electrode (x_6) and positive sign for the current will be assigned to anodic current of the diamond working electrode, i.e., to a flow of positive charge from the diamond to the electrolyte [17]. The voltage source in Fig. 1 for the measurement of the polarization curves was provided by a UNISCAN Model PG580 potentiostat operated in three-electrode configuration with a platinum wire as a counter

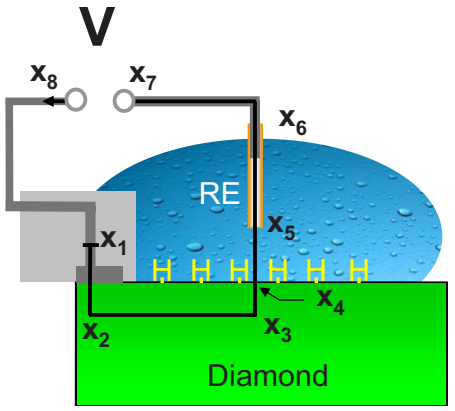

FIG. 1. (Color online) Schematic of the electrical circuit adopted in the experiment. Voltages are given with respect to the reference electrode, i.e., relative to $x_6=x_7$. The path from x_1 to x_8 is the one for which the band diagram is analyzed in Fig. 5.

electrode. For measuring open circuit voltages, the voltage source was replaced by a voltmeter with an internal resistance larger than 10^{12} Ω (Keithley 617 electrometer) or 10^{13} Ω (UNISCAN Model PG580 potentiostat, in the corresponding mode). Both instruments gave the same results. The use of the counter electrode in this case is merely technical in order to speed up equilibration time and protect the reference electrode. Conceptually, all experiments can be understood without considering the counter electrode.

RESULTS

Figure 2 shows the open circuit transients of a hydrogen-terminated diamond electrode as they have been measured as a function of *p*H vs the Ag/AgCl electrode (left-hand scale) for two nominally identical experiments. On the right-hand scale the measured voltages are translated to the SHE as a reference. For the upper panel (a) of the figure, an active area was defined lithographically after sample hydrogenation by masking and plasma oxidation of the remaining part of the surface (sample A); for the lower panel (b) the full rectangular sample surface was used as active area without further structuring (sample B). In both experiments a nonzero cell voltage can clearly be measured that decreases with *p*H. Note that this *p*H dependence is opposite to the *p*H dependence seen in an SGFET configuration when the voltage of constant channel conductivity is monitored ([15], but remember the different sign conventions for the voltage, see [17]). The internal resistance of the galvanic cell is larger than 10^8 Ω and the equilibration time for the electrode after a change of electrolyte *p*H is extremely long, challenging the sensitivity and the stability of the experimental setup.

In experiments on hydrogen-terminated diamond SGFETs a partial oxidation or amination has been found to support if not enable the ion sensitivity of the surface [18,19]. We took these results as a motivation to investigate also the effect of partial oxidation upon the redox activity of the diamond electrode. Figure 3 shows the open circuit transients for a partially oxidized diamond surface for *p*H ranging from 3 to 11. For this experiment the sample has been hydrogenated in the

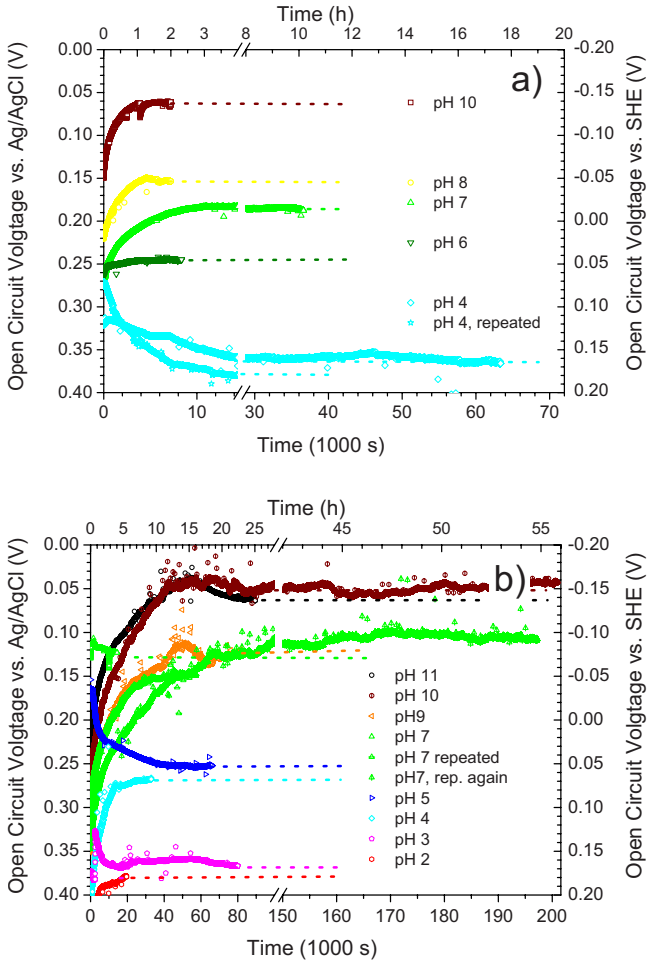

FIG. 2. (Color online) Open circuit voltage transients of a hydrogen-terminated diamond electrode measured vs a Ag/AgCl reference as a function of *p*H. On the right-hand scale, voltages are translated to the standard hydrogen electrode (SHE) potential scale. (a) Sample A: Experiment with a U-shaped conductive channel lithographically defined on the diamond surface. (b) Sample B: Nominally identical experiment using the full square shaped sample surface as active area.

same geometry as for the experiments of Fig. 2(b) and has then been exposed to peroxide (30%) for 30 minutes under simultaneous uv illumination by a mercury discharge lamp (254 nm, 20 W, 3 cm distance unfocused; sample C). Again, open circuit voltages decreasing with *p*H can clearly be measured. Equilibration times are in fact shorter than for sample B [Fig. 2(b)], but comparable with those of sample A [Fig. 2(a)], i.e., for the patterned electrode area that was not intentionally oxidized. We cannot exclude an unintentional slight oxidation of sample A due to imperfect masking during the structuring of the electrode that would explain comparable equilibration times as observed for the intentionally oxidized sample C.

In Fig. 4 we summarize the saturated open circuit voltages as a function of *p*H, and we have also added the corresponding results obtained on a Pt wire electrode in place of the diamond electrode. We see in all cases a negative *p*H sensitivity which is approximately linear within the scatter of the

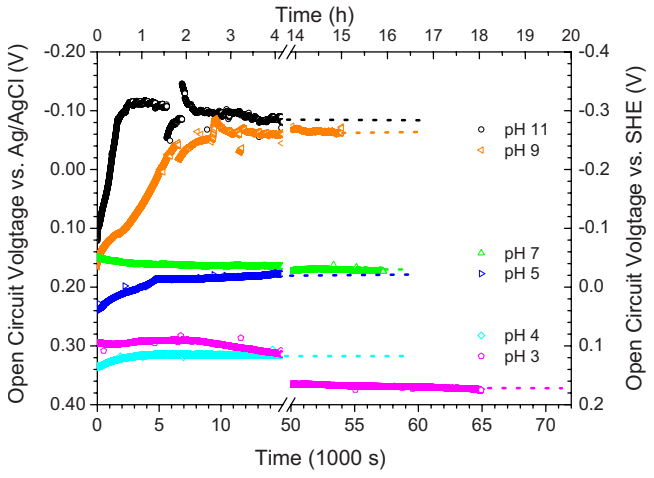

FIG. 3. (Color online) Same as Fig. 2 for a hydrogen-terminated electrode after partial oxidation (sample C).

data. Sensitivity factors range from −40 mV/*p*H for the hydrogen-terminated diamond (samples A and B) to a value apparently consistent with a Nernstian response of −59 mV/*p*H for the partially oxidized diamond electrode (sample C). The *p*H dependence of the hydrogen-hydronium and of the oxygen-hydroxyl redox couples follows Nernst's equation as indicated by the dashed lines in Fig. 4.

For the discussion of our results we adopt the schematic band diagram of the complete electrochemical circuit sketched in Fig. 1, i.e., we consider the electrostatic energy $w(x)$ for a negative unit charge as a function of position x. Two cases belonging to two different voltages are sketched in Fig. 5 and will be discussed below. The same band diagram has already been adopted previously for the discussion of the transfer characteristics and the ion sensitivity of diamond-based SGFETs [15]. Since it illustrates also the essential concepts for the discussion of Faradaic currents and

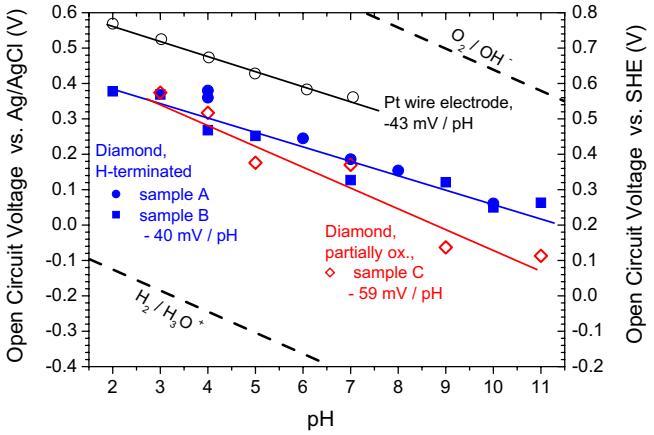

FIG. 4. (Color online) The *p*H dependence of the saturated open circuit voltage for hydrogen-terminated and partially oxidized diamond. For the acidic side, data for a platinum wire electrode are given as well. The dashed lines correspond to the electrochemical potentials of the hydrogen-hydronium and the oxygen-hydroxyl redox couples under atmospheric conditions, respectively.

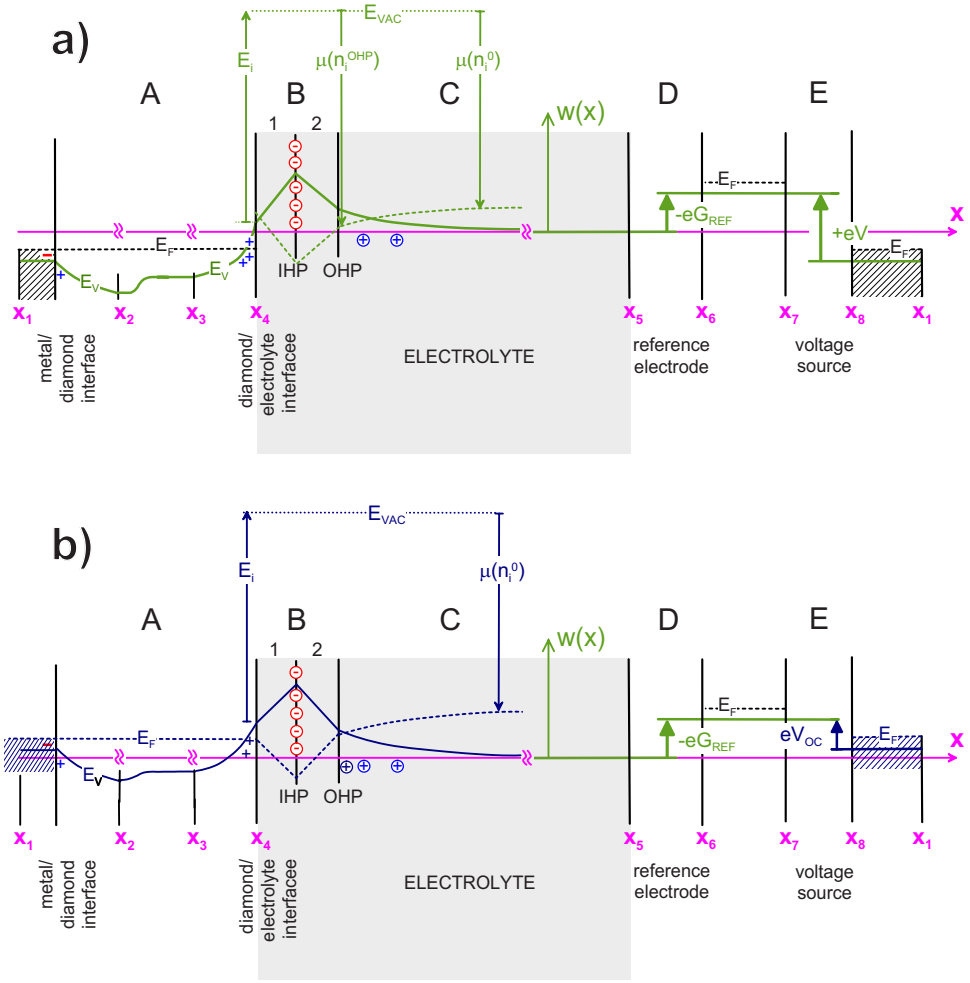

FIG. 5. (Color online) The potential diagram $w(x)$ of the complete galvanic cell used to study the hydrogen-terminated and surface conducting diamond electrode. The potential diagram is constructed along the path defined in Fig. 1 for two different voltages [upper (a) and lower panel (b)] as discussed in the text by approximating the electrode as perfectly polarizable. The dashed line shows the construction of an effective electrochemical potential of the redox electrons of a specific redox couple. The alignment of this electrochemical potential with respect to the Fermi level in the diamond gives the sign of the Faradaic current belonging to the applied voltage V. (a) Represents a potential diagram for an anodic current. In (b) the voltage V has been reduced compared to (a) such that the chemical potential of the redox electrons and the Fermi level just coincide. This situation corresponds to open circuit conditions if only the respective redox couple were active. For further details see text.

the open circuit potential profiles, we will briefly introduce Fig. 5 here again. The circuit consists of A (x_1 to x_4) the diamond working electrode from the metal contact to the free surface exposed to the electrolyte; B, the compact layer consisting of range 1 between the diamond surface and the inner Helmholtz plane (IHP) and of range 2 between the inner and the outer Helmholtz plane (OHP); C (OHP to x_5) the diffuse layer in the electrolyte; D (from x_5 to x_6) the reference electrode including its double layer towards the electrolyte; and E from (x_7 to x_8) the voltage source. The current meter used for measuring the polarization curves can be assumed to be ideal and has no influence on the charge and potential profile. Therefore it has been omitted in Fig. 5. The measurement of open circuit voltages is conceptually equivalent to choosing the voltage such that the current across the diamond-electrolyte interface is zero. We set the potential $w(x)$ deep in the electrolyte where it is asymptotically constant to zero. In part A we choose the valence band maximum (E_v) to show the potential profile in the diamond. In the solid-state parts where the electrical current is carried by electrons (or holes), the Fermi level is indicated by a dashed line. The voltage source results in the same discontinuity eV in both the electrostatic potential and the Fermi level. The reference electrode creates a Galvani potential drop eG_{REF} due to the equilibration of its characteristic redox couple with the electron reservoir of the solid. In the case of the Ag/AgCl reference electrode this is the equilibration of silver ions in the metallic and electrolytic phase, and G_{REF} is the half-cell potential of the electrode. We assume for simplicity that the wiring of the circuit is completely done with silver. In reality, different metals are used but contact potentials in the circuit cancel and therefore need not be considered explicitly in Fig. 5. The sheet charge at the inner Helmholtz plane, that has been exemplarily assumed to be negative in the potential diagram, depends on the ionic composition of the electrolyte. It is this dependence that mainly accounts for the ion sensi-

tivity of the electrode when operated in the SGFET architecture [20,21,23].

The relationship between the voltage applied, $V=\frac{1}{e}[w(x_7)-w(x_8)]$, and the charge density and potential profile can best be understood by considering the potential at the outer Helmhotz plane, w_{OHP}, as a parameter. For a given electrolyte and a given temperature, the total areal (i.e., depth integrated) space charge density in the diffuse layer, σ_{diff}, and with it the electric field at the OHP is a monotonic function of w_{OHP} as expressed by the Grahame equation [22,15]; so is consequently the potential at the IHP. Since the sheet charge density of ions affixed at the IHP, σ_{ads}, is, again for given temperature and electrolyte composition, a well-defined function of this potential only, it is also well defined for a given w_{OHP}. [In the models used so far for a quantitative description of charge and potential profiles of hydrogen-terminated diamond electrodes, [23,15], the simplest functional dependence, i.e., $\sigma_{\mathrm{ads}}(w_{\mathrm{OHP}})=\mathrm{const}$, has been assumed]. We have assumed a negative σ_{ads} here as it is found for $p\mathrm{H}\geqslant 3.5$ for hydrogen-terminated diamond in a recent study by Härtl *et al.* [23]. The choice of negative σ_{ads} is merely for illustration and has no consequences for a principle outline in the following. Taking into account the electric field change induced by σ_{ads} and translating this to the potential $w(x_4)$ at the diamond surface is a trivial task. Charge neutrality requires that the areal hole density p at the diamond side of the interface balances the sum of σ_{diff} and σ_{ads}, and thus p is well defined for a given w_{OHP} as well. p in turn defines the Fermi level at the diamond-electrolyte interface (x_4) relative to the valence band maximum E_v [15,24]. The potential drop inside the diamond is the difference between the valence band maximum E_v at the diamond surface (x_4) and at the diamond-metal interface. Relative to the constant Fermi level, E_v is fixed at the diamond-metal interface and determined by w_{OHP} at the diamond surface x_4. Summarizing, the parameter w_{OHP} allows us to construct the total potential profile in the electrolyte and the diamond part of the circuit and to determine $w(x_1)$. Finally, Kirchoff's loop rule of electrostatics requires the sum of the applied voltage V and the (constant) half-cell potential G_{REF} to be identical to $\frac{1}{-e}w(x_1)$, i.e., $w(x_1)=w(x_8)=-eV-eG_{\mathrm{REF}}$. This fixes the voltage V that belongs to the given w_{OHP}. Exemplarily, we have constructed the potential profile and indicated the space charge density following the arguments outlined above also for another case in Fig. 5. In the lower panel (b) of the figure we have increased the parameter w_{OHP} slightly compared to the upper panel (a) without changing the density σ_{ads} of absorbed ions. As a result, the positive charge in the diffuse layer increases accompanied by an increase in the magnitude of the electric field inside the compact layer. As a consequence $w(x_4)$ increases. On account of charge neutrality, the hole concentration decreases and the Fermi level at x_4 moves up relative to E_v. These two contributions add to an upward shift of E_F in the diagram reducing the voltage V. The comparison of Figs. 5(a) and 5(b) demonstrates the response of the hole density upon variation of the applied voltage. In an SGFET configuration, it is directly proportional to the transfer characteristics of the device in the limit of small source-drain voltage as discussed extensively in Ref. [15].

So far no electron exchange across the diamond-electrolyte interface, i.e., no Faradaic current, has been considered. This shall be done now. In general, more than one redox couple will be present in the electrolyte and thus the total electric current is the sum of partial currents, each assigned to an individual redox couple. For aqueous electrolytes in contact with atmosphere, at least the hydrogen-hydronium and the oxygen-hydroxyl couples already mentioned must be considered. The driving force of the partial currents assigned to them is not the gradient of the electrostatic potential plotted in Fig. 5 but it is the difference in the electrochemical potential of the redox electrons on either side of the compact layer. Since the diamond-electrolyte interface constitutes by far the highest resistance in the circuit of Fig. 1, the Faradaic current is carried through the rest of the circuit with negligible deviation from the equilibrium potential profile discussed so far. On the diamond side, the electrochemical potential of the electrons is the Fermi level E_F that is determined relative to E_V by the hole concentration [24]. Since the ionization energy $E_i=E_{\mathrm{VAC}}-E_V$ of hydrogen-terminated diamond is a fixed parameter of the electrode, we can construct the vacuum level E_{VAC} as a reference for the chemical potential of redox electrons as it is indicated by the dotted lines in Fig. 5. On the electrolytic side, the electrochemical potential $\bar{\mu}$ needs to be evaluated for each redox couple separately. Let us exemplarily consider the contribution I_{H_2} of the hydrogen-hydronium couple to the total Faradaic current I. The chemical potential μ^{OHP} relative to E_{VAC} at the OHP of the redox electrons in the electrolyte corresponding to this redox couple is determined via Nernst's equation by the concentrations of the redox active species at the OHP,

$$\mu^{\mathrm{OHP}}=\mu(n_{\mathrm{H_3O^+}}^{\mathrm{OHP}})=\mu_{\mathrm{SHE}}-kT\ln\left(\frac{n_{\mathrm{H_3O^+}}^{\mathrm{OHP}}}{1\ \mathrm{mole/l}}\right)+\frac{kT}{2}\ln\left(\frac{[\mathrm{H_2}]^{\mathrm{OHP}}}{[\mathrm{H_2}]_{\mathrm{SHE}}}\right). \quad (1)$$

$\mu_{\mathrm{SHE}}=-4.44$ eV is the chemical potential of the standard hydrogen electrode with respect to the vacuum energy. $n_{\mathrm{H_3O^+}}^{\mathrm{OHP}}$ is the molar proton concentration at the OHP, and $[\mathrm{H_2}]^{\mathrm{OHP}}$ and $[\mathrm{H_2}]_{\mathrm{SHE}}$ are the concentrations of dissolved hydrogen in the electrolyte and in the standard hydrogen electrode, respectively. Across the diffuse layer the concentration of the redox active ions is exponentially increasing or decreasing with $w(x)$ for positive or negative valency, respectively. This holds as long as mass transport is not the limiting step for the electrode reaction under consideration. Specifically, we have

$$n_{\mathrm{H_3O^+}}^{\mathrm{OHP}}=n_{\mathrm{H_3O^+}}^{0}\exp\left(\frac{w_{\mathrm{OHP}}}{kT}\right) \quad (2)$$

for the hydronium profile. $n_{\mathrm{H_3O^+}}^{0}$ is the $\mathrm{H_3O^+}$ concentration in the bulk of the electrolyte where $w(x)=0$. Inserting (2) into (1) shows that the chemical potential $\mu(n_i^{\mathrm{OHP}})$ can also be calculated by using the asymptotic bulk concentrations n_i^0 of the redox ions to obtain $\mu(n_i^0)$ and by subtracting the potential w_{OHP}. We use the general index i instead of $\mathrm{H_3O^+}$ here to indicate that in principle all charged constituents of the redox couple change their concentration across the diffuse layer.

Finally, the influence of the electrostatic potential difference between the valence band electrons at the diamond surface and the redox electrons at the OHP on the electron exchange must be taken into account as well. This is done by adding $w_{\mathrm{OHP}}-w(x_4)$ to μ^{OHP} in order to obtain the electrochemical potential $\bar{\mu}^{\mathrm{OHP}}=\mu(n_i^0)-w(x_4)$. This construction for the electrochemical potential of the redox electrons by adding the negative of the electrostatic potential to $\mu(n_i^0)$ is shown by the dashed line in Fig. 5. In the upper panel (a) it yields $\bar{\mu}^{\mathrm{OHP}}$ (the dashed line at x_4) above the Fermi level corresponding to an anodic Faradaic partial current for the redox couple under consideration. In the lower panel (b) the voltage is chosen (by the parameter w_{OHP}) such that $\bar{\mu}^{\mathrm{OHP}}=E_F$. This specific voltage V_{OC} is the one for which the partial Faradaic current I_{H_2} of the hydrogen couple vanishes i.e., for which $I_{\mathrm{H}_2}=0$. If only the hydrogen redox couple were active at the diamond-electrolyte interface, this would be the open circuit voltage vs the chosen reference electrode that resulted from the equilibration of the working electrode with the hydrogen-hydronium redox couple. Following this line of arguments one might at first glance expect the open circuit voltage V_{OC} to depend on the ionization energy E_i of the diamond electrode that was used to position the vacuum level in the energy diagram. Considering the potential drop $w(x_1)-w(x_4)$ in the diamond and evaluating the half-cell potential G_{REF} of the reference electrode in terms of work function and chemical potential differences shows, however, that the properties of the electrode cancel and the open circuit voltage is in fact just the difference between the redox potentials of the reference electrode and of the redox couple under consideration at the diamond electrode [25]. This is, of course, the general expression for the open circuit voltage of a galvanic cell with these two redox couples. For the hydrogen-hydronium redox couple the standard redox potential is $P=0.00$ V on the SHE scale by definition. Correcting for the real concentrations of H_3O^+ and dissolved hydrogen molecules in the electrolyte according to Nernst's equation (1) we find $P_{\mathrm{H}_2}=-0.22$ V corresponding to $\mu_{\mathrm{H}_2}(n_i^0)=-4.22$ eV for pH7. For the hydrogen concentration $[\mathrm{H}_2]/[\mathrm{H}_2]_{\mathrm{SHE}}=5.5\times10^{-7}$ was assumed corresponding to 0.55 μbar for the partial pressure of H_2 in atmosphere which appears to hold universally [26]. By the same procedure we find the redox potential $P_{\mathrm{O}_2}=+0.81$ V and $\mu_{\mathrm{O}_2}(n_i^0)=-5.25$ eV for the oxygen-hydroxyl redox couple in aqueous solution in contact with atmosphere and at pH7. Corresponding to the partial pressure of oxygen in atmosphere, the oxygen concentration has been assumed to be 21% of that for the standard oxygen electrode. When referenced to the right hand scale, the two dashed lines in Fig. 4 thus correspond to $P_{\mathrm{O}_2}=+0.81$ V-0.059 V $(p\mathrm{H}-7)$ and $P_{\mathrm{H}_2}=-0.22$ V-0.059 V $(p\mathrm{H}-7)$. As outlined above, these potentials are identical to the open circuit voltages expected when the working electrode were in equilibrium with the respective redox couple only. They are denoted as their reversible potentials. The experimental results for V_{OC} lie in all cases in between. As a straightforward conclusion, both the hydrogen-hydronium and the oxygen-hydroxyl redox couple obviously determine the charge transfer equilibrium at the diamond-electrolyte interface, and the open circuit potential

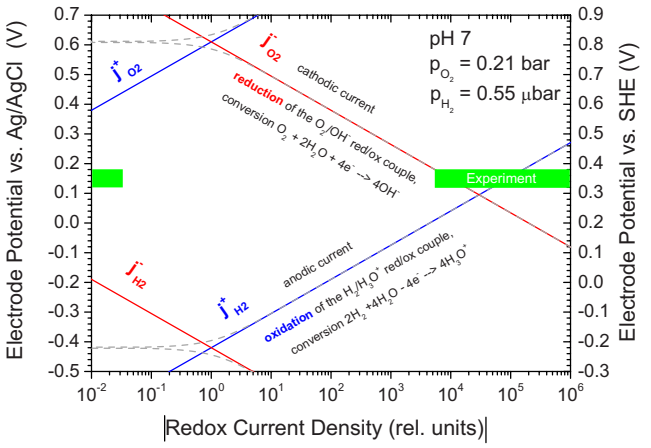

FIG. 6. (Color online) Schematic Evans diagram for simultaneous redox activity of the hydrogen-hydronium and the oxygen-hydroxyl redox couples in an electrolyte at pH7 and in contact with atmosphere. The range of open circuit voltages observed at pH7 (Figs. 2 and 3) is indicated by the horizontal bar labeled "Experiment."

measured is a mixed potential. This situation is typically found in the electrochemistry of corrosion where one of the two redox couples involves the electrode material itself, and the mixed potential is also called corrosion potential [27]. Although diamond is perfectly inert in these experiments and does not corrode, the concepts of corrosion science are helpful to understand the situation here as well. In Fig. 6 we have schematically constructed for pH7 a so-called Evans diagram usually adopted for the discussion of corrosion potentials [28,29]. On the logarithmic abscissa the Faradaic current densities $j_{\mathrm{H}_2}=I_{\mathrm{H}_2}/A$ and $j_{\mathrm{O}_2}=I_{\mathrm{O}_2}/A$ are shown with their respective anodic (j^+, blue) and cathodic (j^-, red) contributions as a function of the applied voltage. For a given redox couple, j^+ and j^- cancel exactly when the voltage applied to the working electrode is identical to the reversible potential P of the corresponding redox couple (–0.22 V vs SHE for the H_2 and +0.81 V vs SHE for the O_2 couple). Obviously, these conditions can be fulfilled for the hydrogen-hydronium or for the oxygen-hydroxyl redox couples separately, but never for both simultaneously. The functional form of the partial current densities in Fig. 6 has been schematically assumed to follow the Butler-Volmer relation [30]

$$j_k = j_{0,k}\left[\exp\left(\frac{\alpha_k(V-P_k)e}{kT}\right)-\exp\left(-\frac{(1-\alpha_k)(V-P_k)e}{kT}\right)\right] \tag{3}$$

with the transfer coefficient α_k, the reversible potential P_k and the reversible exchange current density $j_{0,k}$. Each of these quantities is specific for the redox couple under consideration denoted here by the index k, and $j_{0,k}$ and α depend on the electrode material as well. This relation is usually valid as long as the "overpotential" $|V-P_k|$ is low enough to guarantee that the electron exchange across the electrode-electrolyte interface is the limiting step for the Faradaic current. For higher overpotentials, the diffusive transport of redox particles to the electrode interface in general becomes

the limiting process, and the polarization curves $j_k(V)$ saturate. In Fig. 6 we have neglected this effect. Following the Butler-Volmer relation (3), the anodic and cathodic partial current densities thus give straight lines in the Evans diagram. Inside the voltage range defined by $e(P_{O_2}-V) \gg kT/\alpha_{O_2}$ and $e(V-P_{H_2}) \gg kT/(1-\alpha_{H_2})$ only the anodic current corresponding to the oxygen-hydroxyl redox couple and the cathodic current of the hydronium-hydrogen redox couple need to be considered. This voltage range will be denoted as the corrosion window in the following. In Fig. 6 it extends from about −0.15 V to 0.75 V vs SHE. Open circuit conditions require that the cathodic and the anodic current densities cancel, and thus the intersection of the current curves in the corrosion window defines the open circuit voltage V_{OC}. For the schematic of Fig. 6 we have set $\alpha_{H_2}=\alpha_{O_2}=0.5$ and $j_{0,H_2}=j_{0,O_2}$, and thus $V_{OC}=(P_{H_2}+P_{O_2})/2$, i.e., the corrosion potential is the average of the two reversible potentials of the two redox couples involved. This specific result, of course, depends on our simplifying assumption of identical reversible exchange current densities and of transfer coefficients adding to one. It is thus coincidental that the experimental range of OCV's measured at *p*H7 is almost consistent with $V_{OC}=(P_{H_2}+P_{O_2})/2=0.30$ V vs SHE (0.36 ± 0.03 V vs SHE, compare Fig. 4).

Before discussing the *p*H dependence of the OCV we would like to comment on the mixed potential observed here in the framework of real corrosion phenomena. The reader may, for example, replace the oxygen redox couple by one that corresponds to the corrosion of an ignoble metal electrode, say $Fe \rightleftarrows Fe^{2+}+2e^-$ with $[Fe^{2+}]=5\times10^{-6}$ moles/l which has a reversible potential $P_{Fe}=-0.60$ V vs SHE. In an Evans diagram this redox couple lies below the hydrogen-hydronium one. At the corrosion potential, i.e., under open circuit conditions, the zero electrical current implies a cathodic partial current of the hydrogen-hydronium redox couple balancing an anodic partial current of same magnitude of the iron couple. The consequence is the corrosion reaction of iron under hydrogen evolution with the reaction rate corresponding to the reaction current density read from the Evans diagram. Going back to our case of the mixed potential of the hydrogen-hydronium and the oxygen-hydroxyl couple, we see that the corrosion reaction in this case is not involving the electrode, but is the water synthesis from oxygen and hydrogen. In fact, it does not even require an electrical circuit but just an electrode surface providing and consuming electrons at the rate of the exchange current. Under the open circuit conditions studied, i.e., for a hydrogen-terminated diamond electrode in an aqueous solution in contact with atmosphere, we thus observe a charge transfer equilibrium witnessed by the nonzero cell potential vs our reference electrode that corresponds to a persistent production of water from the oxygen and hydrogen reservoir of the atmosphere. Electrons are exchanged with the hydrogen-hydronium and the oxygen-hydroxyl redox couples at the same rate. This amazing result will be elaborated on further below.

Within the corrosion window, the total current density is easily evaluated from Eq. (3) as

$$j = j_0\left[\exp\left(\frac{\alpha\eta e}{kT}\right) - \exp\left(-\frac{\beta\eta e}{kT}\right)\right], \tag{4}$$

i.e., again a Butler-Volmer-type relation with the overpotential $\eta=V-V_{OC}$ now referenced to the mixed potential V_{OC} and the reaction current density j_0 replacing the reversible exchange current densities. $\alpha=\alpha_{H_2}$ stands for the transfer coefficient of the hydrogen reaction and $\beta=1-\alpha_{O_2}$ for the complement of the transfer coefficient of the oxygen reaction. Note, that in general the prefactors in the exponent do no longer add up to 1, (i.e.), $\alpha+\beta\neq1$. Evaluating Eq. (3) for both the hydrogen and the oxygen reaction inside the corrosion window, and requiring $j_{H_2}(V_{OC})=-j_{O_2}(V_{OC})$, gives by straightforward calculus

$$V_{OC} = \left(\frac{\alpha}{\alpha+\beta}P_{H_2} + \frac{\beta}{\alpha+\beta}P_{O_2}\right) - \frac{kT}{e}\times\frac{\ln(j_{0,H_2}/j_{0,O_2})}{\alpha+\beta}. \tag{5}$$

The first term on the right-hand side is a weighted average of the reversible potentials of the two redox couples involved, where the weighing factors are the relative transfer coefficients. The second term takes the generally different reversible exchange current densities into account.

We will discuss the *p*H dependence of the mixed potential on the basis of Eq. (5). If we assume, as the simplest approximation, that the reaction kinetics of the hydrogen and the oxygen reaction are independent of *p*H, the reversible exchange current densities and the transfer coefficients in Eq. (5) are constant. A variation of the proton concentration is then taken into account by the *p*H dependence of P_{H_2} and P_{O_2} as given by Nernst's equation and as already discussed above. The open circuit voltage, i.e., the corrosion potential, is then to follow the same *p*H shift of −59 mV/*p*H. Assuming *p*H independent kinetics is, however, a rather crude assumption, and it comes not as a surprise that the experimental *p*H dependence of Fig. 4 is deviating from the Nernstian expectation. This deviation can be due to a *p*H dependence of either one of the reversible exchange current densities and transfer coefficients or to a combination of several of them. For a further analysis, the polarization curves for both redox couples must be measured independently. We stress explicitly here, however, that the Nernst value for the *p*H dependence of the mixed potential is not a canonical one, and not even a limit. Depending on the sign and magnitude of *p*H shifts of j_{H_2}/j_{O_2} and of the transfer coefficients α and β, the slope of the *p*H curves in Fig. 4 can be smaller, but also larger than −59 mV/*p*H. We further note in passing, that the *p*H dependence of the platinum wire electrode is also deviating from −59 mV/*p*H, certainly for the same kinetic reasons as discussed above in general terms. Hence, using a simple wire electrode as reference in an electrochemical experiment induces *p*H dependent voltage shifts that are notoriously uncontrollable [31].

So far we have described both the hydrogen and the oxygen reaction by the Butler-Volmer equation (3) within the corrosion window, implicitly assuming that the reaction rate is controlled by the charge transfer of redox electrons across

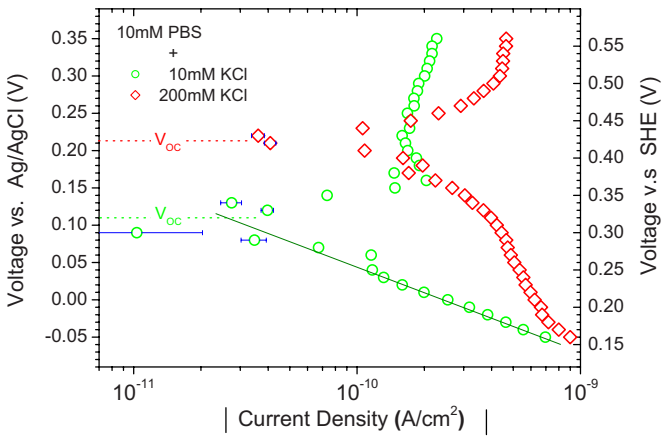

FIG. 7. (Color online) Quasi static polarization curves (*I-V* diagrams) in the vicinity of the open circuit voltage V_{OC} for a standard electrolyte at *p*H7 and one with a high concentration of KCl (0.2 moles/l). For details see text.

the diamond-electrolyte interface. The polarization curve, i.e., the *I-V* characteristics of the galvanic cell formed by the hydrogen and the oxygen redox couples active at the diamond electrode side and of the Ag/AgCl redox couple of the reference electrode, is thus expected to follow Eq. (4). In order to interpret the polarization curve along those lines, transient and mass transport effects associated with the redox half-reactions must be suppressed. We have therefore measured the polarization curve for two *p*H7 electrolytes in the quasistatic mode (Fig. 7). Voltage set points were selected manually, and the transients of the current in the reference electrode circuit were monitored for at least 20 minutes until saturation was reproductively achieved. The error bars shown together with the open symbol data points are the standard deviation (RMS) of the current in the steady state. We had to use the quasistatic mode of operation because dynamic voltammetry turned out to be inappropriate even with voltage scan rates as low as 0.05 mV/s. The open circles in Fig. 7 were measured according to our standard conditions, i.e., for a 10 mM PBS buffer at *p*H7 with 10 mM KCl added as additional background electrolyte. We observe a zero crossing of the quasistatic polarization curve at $V=V_{OC}=+0.11$ V vs Ag/AgCl, consistent with Figs. 2 and 4. On the cathodic side (lower voltages), the current is preferentially due to the oxygen reaction $O_2+2H_2O+4e^- \rightarrow 4OH^-$, and for $|V-V_{OC}| \geqslant 50$ mV it follows faithfully the Butler-Volmer relation with a slope of $\beta=0.50\pm0.05$. Similar behavior is found for most metal electrodes studied so far [32,33]. We take this as strong evidence that the oxygen reaction is charge-transfer limited in the entire range from its reversible potential up to the corrosion potential. Extrapolating the cathodic current density to the voltage of zero current V_{OC} yields $j_0=3.0\times10^{-11}$ A/cm^2 for the reaction current density under open circuit conditions. Thus, a hydrogen terminated diamond surface in contact with water under atmospheric conditions catalytically mediates the water synthesis reaction $O_2+2H_2 \rightarrow 2H_2O$ with an areal rate of $j_0/(2e)=9.4\times10^7$ cm^{-2} s^{-1}, corresponding to 1.6×10^{-16} moles cm^{-2} s^{-1}. Although this reaction rate can clearly be measured electrochemically and proves the redox activity of the diamond surface under atmospheric conditions, it is minute in terms of material transformation. Using the molar density of water (0.055 moles/cm^3) one may translate this reaction rate to the growth rate of a water layer, the result being 2.9×10^{-15} cm/s$\approx$1 nm/year. Despite this ridiculously low reaction rate the electron transfer associated with it is in perfect agreement with the kinetics of surface transfer doping under atmospheric conditions. Taking j_0 as an estimate for an electron exchange current density across the diamond surface driven with a chemical potential difference of 0.5 eV gives a generation rate of 2×10^8 holes cm^{-2} s^{-1}. It will thus take about 3 hours to induce a typical hole density of 2×10^{12} holes/cm^2. Such transients, sometimes even with longer saturation times, are in fact observed for the appearance of surface conductivity of hydrogen-terminated diamond under atmospheric conditions [1,3]. We explicitly stress here that the exchange current densities measured in this experiment correspond to a solid-liquid interface and can thus only yield a rough estimate for the time scale on which surface conductivity is generated in atmosphere. The real charge exchange of the surface transfer doping mechanism involves only a thin water layer, and reaction kinetics can be substantially different, probably faster, under those conditions on which surface conductivity is generated in atmosphere.

On the anodic side ($V>V_{OC}$) the Faradaic current is predominantly carried by the hydrogen reaction $H_2+2H_2O \rightarrow 2H_3O^+ + 2e^-$. The polarization curve is clearly deviating here from the Butler-Volmer behavior, indicating a saturation of the current. Such saturation is expected when the reaction becomes mass transport limited, and the data here obviously constitute the transition between electrode reaction and diffusion limitation (mixed control). For the case at hand, the diffusion of hydrogen to the diamond surface must be considered. The hydrogen partial pressure in atmosphere equals 5.5×10^{-7} bar [26], which corresponds to a molecular density of dissolved hydrogen $n_{H_2}=2.9\times10^{11}$ cm^{-3} [34]. With a room-temperature diffusion constant of $D_{H_2}=5\times10^{-5}$ cm^2/s [35] and a typical extension of the diffusion layer between $\ell=10^{-3}$ cm and $\ell=10^{-2}$ cm [36,37], the maximum diffusion current density $r_{H_2}=n_{H_2}D_{H_2}/\ell$ for H_2 molecules lies between 1.5×10^9 and 1.5×10^{10} cm^{-2} s^{-1}. This corresponds to electrical current densities $j_{H_2}=2er_{H_2}$ between 5×10^{-10} and 5×10^{-9} A/cm^2. This rough estimate is consistent with the data of Fig. 7. An extrapolation of the anodic current density corresponding to Eq. (5) is no longer possible in the case of mixed control. Note that, due to the $\sim10^6$ times higher partial pressure of oxygen in air and thus of dissolved oxygen in the electrolyte, the diffusion limited current density on the cathodic side is never reached in the experiment.

We have discussed the hydrogen-hydronium redox couple fixing the mixed potential on the low potential side (Figs. 6–8) by providing the anodic current that compensates the cathodic one due to the oxygen-hydroxyl couple. In view of the small concentration of dissolved hydrogen in the electrolytes this raises the question wether alternative redox couples based on other trace gases in the atmosphere could equally

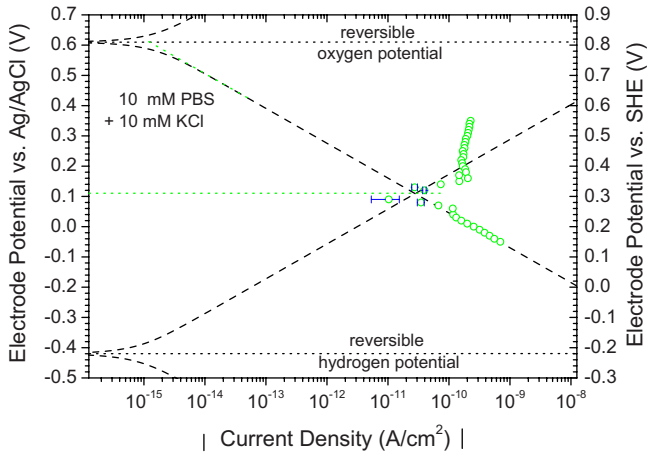

FIG. 8. (Color online) Plot of the *I-V* data of Fig. 7 (standard electrolyte) in an Evans diagram covering the complete corrosion window between the oxygen and the hydrogen reaction.

well take that role. Candidates that come to mind are, for example, N_2O, NO_2, or SO_2. They all form redox couples with hydonium and acidic anions or with undissolved acid molecules [38]. When the corresponding redox potential falls into the corrosion window displayed in Fig. 6 below the experimentally observed corrosion potential one may expect it to replace the hydrogen-hydronium couple. We will discuss such a scenario exemplary for NO_2. This molecule forms a redox couple with hydronium and NO_3^-, the anion of the nitric acid, with the redox half-reaction being $NO_2+3H_2O \rightleftharpoons NO_3^-+2H_3O^++e^-$ and a standard potential of $P^0=+0.81$ V vs SHE [38]. Comparing this half-reaction with that of the hydrogen-hydronium couple, $H_2+2H_2O \rightleftarrows 2H_3O^++2e^-$, it promises to be a reasonable substitution at first glance. It may even be tempting to evaluate its redox potential for *p*H7 via the Nernst correction. One obtains $P=-0.02$ V, i.e., a value right inside the corrosion window and below the experimental corrosion potential of 0.35 ± 0.04 V vs SHE. However, and in contrast to the hydrogen-hydronium couple, the NO_2 half-reaction can be balanced by the concentration of NO_3^- as a further redox ion participating in the equilibrium. Thus, this couple is not potential fixing, but instead it follows the potential adjusted by the redox couples discussed above. The same arguments hold for the other trace gases mentioned above. We can thus exclude them from a further discussion.

The only trace element in air for which such reasoning does not hold is ozone with concentrations of about 50 ppb. The corresponding redox half-reaction is $O_2+3H_2O \rightleftharpoons O_3+2H_3O^++2e^-$ with a standard potential of $P^0=+2.07$ V [38]. In this case all relevant concentrations that determine the redox potential are fixed with *p*H and with the partial pressure of oxygen and ozone in the atmosphere. Using the ozone concentration of 50 ppb mentioned above, a partial pressure of oxygen of 210 mbar and *p*H7 yields a redox potential of $P^0=1.7$ V vs SHE. This value is, however, clearly above the oxygen-hydroxyl couple, i.e., outside the corrosion window relevant here.

The second data set in Fig. 7 (open diamonds) has been measured in an electrolyte with a 20-fold higher concentration of KCl. We were motivated to study the effect of increasing halogen ion concentration by experiments on SGFETs by the current authors and others showing a pronounced increase of Faradaic currents with increasing iodine and chlorine ion concentrations. [See, for example, I_{ds} vs V_{gs} for $V_{ds}=0$ in Fig. 2 of Ref. [39]; this current is in fact a Faradaic (gate) current such as we discuss here.] We thus expect a major change in the redox kinetics with halogen concentration that is confirmed in Fig. 7. Kanazawa *et al.* [39] ascribe the effect of chloride ions on their ISFET characteristics as due to a specific adsorption of Cl^- in the Helmholtz layer. The open circuit voltage shifts by 0.10 V, and the cathodic and anodic current densities are clearly higher than before. Both the cathodic and the anodic current densities moreover do no longer follow the Butler-Volmer relation, all indicating that chlorine ions have a major impact on the charge transfer of electrons at the diamond-electrolyte interface. This issue is subject of on-going research work.

For low concentrations of KCl, the cathodic part of the polarization curve may even be extrapolated to the reversible potential of the oxygen reaction at $P=+0.81$ V vs SHE. The result is shown in Fig. 8 in an Evans diagram similar to the schematic one of Fig. 6. The back extrapolation of the cathodic current with a transfer factor of $\beta=0.5$ yields a reversible exchange current density of $j_{0,O_2}\approx 1\times10^{-15}$ A/cm^2 for the oxygen-hydroxyl redox couple at the hydrogen-terminated diamond surface. As explained above, the anodic current due to the hydrogen-hydronium couple is apparently not reaction controlled, and a back extrapolation can only be interpreted with great caution. The corresponding current density for the open circuit voltage can, however, be taken from the reaction current density. Extrapolating back from that value (+0.11 V and 3×10^{-11} A/cm^2) with $\alpha=0.5$ would give a reversible exchange current density of $j_{0,H_2}\approx 7\times10^{-16}$ A/cm^2. Although this value should only be taken as a very rough estimate it is yet interesting to note that it is within a factor of 2 identical with j_{0,O_2}.

CONCLUSION

We have studied the electron exchange between hydrogen-terminated diamond electrodes and aqueous electrolyte in which the active redox couples were restricted to hydrogen-hydronium and oxygen-hydroxyl.

The redox activity of the electrode was witnessed by a *p*H-dependent cell voltage vs Ag/AgCl between −0.1 V (*p*H11) and +0.4 V (*p*H2) varying between 11 and 2. *p*H sensitivities between −40 mV/*p*H and −59 mV/*p*H were measured depending on sample surface conditions. In all cases the cell potentials (open circuit voltage) were in between those expected for a situation where either the H_2/H_3O^+ or the O_2/OH^- redox couple were active alone. Hence, the open circuit voltage is determined by the balance of an anodic current due to hydrogen oxidation on the one side ($H_2+2H_2O-2e^-\rightarrow 2H_3O^+$) and a cathodic current due to the reduction of oxygen on the other side ($O_2+H_2O+2e^-\rightarrow 4OH^-$). The corresponding mixed potential is recognized as the classical corrosion potential in electrochemistry. However, whereas corrosion normally leads to

the decomposition of the electrode material the diamond is left intact in our case and the corrosion reaction corresponds to water synthesis from H_2 and O_2 catalytically mediated by the diamond surface. The analysis of the quasistatic polarization curve measured for *p*H7 shows a charge-transfer-limited current for the oxygen-hydroxyl couple at least up to an overpotential of 0.65 V with an extremely low reversible exchange current density of 10^{-15} A/cm^2. On the other hand, the anodic current due to the hydrogen-hydronium couple saturates already for voltage exceeding the open circuit voltage by 0.1 V.

The principles used here to describe open circuit conditions hold as well for free diamond surfaces in contact with electrolyte or with humid air. Therefore, contrary to what has been claimed so far, it is neither the hydrogen-hydronium couple [1] nor the oxygen-hydroxyl couple [6] alone that determines the hole accumulation layer of surface conductive diamond. The extremely low exchange current densities of the order of 10^{-15} A/cm^2 account quantitatively for the long-time constants needed to establish a saturated surface conductivity on diamond after exposure to air.

ACKNOWLEDGMENT

This work was financially supported by the EU FP6 Marie Curie Research Training Network "DRIVE" (Contract No. MRTN-CT-2004-512224).

[1] F. Maier, M. Riedel, B. Mantel, J. Ristein, and L. Ley, Phys. Rev. Lett. **85**, 3472 (2000).
[2] S. G. Ri *et al.*, Jpn. J. Appl. Phys., Part 1 **38**, 349 (1999).
[3] J. Foord, C. H. Lau, M. Hiramatsu, R. B. Jackman, C. E. Nebel, and P. Bergonzo, Diamond Relat. Mater. **11**, 856 (2002).
[4] J. J. Mares, P. Hubik, J. Kristofik, J. Ristein, P. Strobel, and L. Ley, Diamond Relat. Mater. **17**, 1356 (2002).
[5] R. Müller, A. Denisenko, and E. Kohn, Diamond Relat. Mater. **12**, 554 (2003).
[6] V. Chakrapani, J. C. Angus, A. B. Anderson, S. C. Wolter, B. R. Stoner, and G. U. Sumanasekera, Science **318**, 1424 (2007).
[7] J. Ristein, Science **313**, 1057 (2006).
[8] H. Kawarada, M. Aoki, and M. Ito, Appl. Phys. Lett. **65**, 1563 (1994).
[9] P. Gluche, A. Aleksov, A. Vescan, W. Ebert, and E. Kohn, IEEE Electron Device Lett. **18**, 547 (1997).
[10] H. Umezawa, K. Tsugawa, S. Yamanaka, d. Takeuchi, D. Okushi, and H. Kawarada, Jpn. J. Appl. Phys., Part 2 **38**, L1222 (1999).
[11] H. Kawarada, Y. Araki, T. Sakai, T. Ogawa, and H. Umezawa, Phys. Status Solidi A **185**, 79 (2001).
[12] B. Rezek, H. Watanabe, D. Shin, T. Yamamoto, and C. E. Nebel, Diamond Relat. Mater. **15**, 673 (2006).
[13] A. Denisenko, A. Aleksov, and E. Kohn, Diamond Relat. Mater. **10**, 677 (2001).
[14] M. Dankerl, A. Reitinger, M. Stutzmann, and J. A. Garrido, Phys. Status Solidi (RRL) **2**, 31 (2008).
[15] J. Ristein, W. Zhang, and L. Ley, preceding paper, Phys. Rev. E **78**, 041602 (2008).
[16] M. Riedel, J. Ristein, and L. Ley, Phys. Rev. B **69**, 125338 (2004).
[17] In Ref. [15] we have discussed the hydrogenated diamond electrode when involved in a SGFET architecture. In that case the voltage between the working electrode and the reference electrode was used as a gate voltage V_{GS} for the transistor. Following common use of device physics this gate voltage was in that work defined with opposite sign as the voltage V of the working electrode here.
[18] T. Sakai, K.-S. Song, H. Kanazawa, Y. Nakamura, H. Umezawa, M. Tachiki, and H. Kawarada, Diamond Relat. Mater. **12**, 1971 (2003).
[19] K.-S. Song, Y. Nakamura, Y. Sakai, M. Degawa, J.-H. Yang, and H. Kawarada, Anal. Chim. Acta **573-574**, 3 (2006).
[20] H. Kanazawa, K.-S. Song, T. Sakai, Y. Nakamura, H. Umezawa, M. Tachiki, and H. Kawarada, Diamond Relat. Mater. **12**, 618 (2003).
[21] T. Sakai, Y. Araki, H. Kanazawa, H. Umezawa, M. Tachiki, and H. Kawarada, Jpn. J. Appl. Phys., Part 1 **41**, 2595 (2002).
[22] D. C. Grahame, Chem. Rev. (Washington, D.C.) **41**, 441 (1947).
[23] A. Härtl, J. A. Garrido, S. Nowy, R. Zimmermann, C. Werner, D. Horinek, R. Netz, and M. Stutzmann, J. Am. Chem. Soc. **129**, 1287 (2007).
[24] J. Ristein, J. Phys. D **39**, R71 (2006).
[25] Let the u_s be the energy of E_v relative to E_F at x_4 and u_{me} correspondingly at the diamond-metal interface. Obviously then, $w(x_1)-w(x_4)=u_{me}-u_s$. Since the metal contact is equilibrated with the diamond valence band, u_{me} is related to the work function Φ_{me} of the metal and the ionization energy E_i of the diamond as $u_{me}=\Phi_{me}-E_i$. From both $w(x_1)=w(x_4)+\Phi_{me}-E_i-u_s$. From Fig. 5(b), i.e., for the specific case of open circuit voltage, $w(x_4)$ is read off as $w(x_4)=+E_i+u_s+\mu(n_i^0)$. Inserting this into the expression for $w(x_1)$ yields $w(x_1)=\Phi_{me}+\mu(n_i^0)$. Kirchhoff's loop rule gives on the other hand $w(x_1)=-eG_{\mathrm{REF}}-eV_{\mathrm{OC}}$, thus $eV_{\mathrm{OC}}=-eG_{\mathrm{REF}}-\mu(n_i^0)-\Phi_{me}$. The half-cell potential $eG_{\mathrm{REF}}=w(x_5)-w(x_6)$ is the difference between the chemical potential μ_{Ag^+} of the redox electrons of the silver ions of the reference electrode and of the electrons in the metal phase of the reference electrode $\mu_{\mathrm{Ag}}=-\Phi_{\mathrm{Ag}}$. Thus $-eG_{\mathrm{REF}}=\mu_{\mathrm{Ag}^+}+\Phi_{\mathrm{Ag}}$. Finally with this $eV_{\mathrm{OC}}=\Phi_{\mathrm{Ag}}-\Phi_{me}+\mu_{\mathrm{Ag}^+}-\mu_e(n_i^0)$ results. The difference in the two metal work functions is zero when Ag is used for the wiring of the circuit exclusively, or compensates with further contact potentials otherwise so that finally $eV_{\mathrm{OC}}=\mu_{\mathrm{Ag}^+}-\mu(n_i^0)$ results.
[26] NASA Earth Fact Sheet, http://nssdc.gsfc.nasa.gov/planetary/factsheet/earthfact.html
[27] L. L. Shreir, R. A. Jarman, and G. T. Burstein, *Corrosion*, 3rd ed., Vol. 1: Metal/environment reactions (Butterworth-

Heinemann, London, 1994), pp. 1:92–1:113.
[28] U. R. Evans and T. P. Hoar, Trans. Faraday Soc. **30**, 424 (1934).
[29] M. Stern and A. L. Geary, J. Electrochem. Soc. **104**, 56 (1957).
[30] R. Memming, *Semiconductor Electrochemistry* (Wiley VCH, Weinheim, 2001), p. 155.
[31] N. Miura, G. Lu, and N. Yamazoe, Solid State Ionics **136-137**, 533 (2000).
[32] K. Kinoshita, *Electrochemical Oxygen Technology* (Wiley-Interscience, New York, 1992), pp. 36–38.
[33] H. Kaesche, *Corrosion of Metals: Physicochemical Principles and Current Problems* (Springer, Berlin, 2003), p. 92.
[34] D. A. Wiesenburg and N. L. Guinasso, Jr., J. Chem. Eng. Data **24**, 356 (1979).
[35] D. M. Himmelblau, Chem. Rev. (Washington, D.C.) **64**, 527 (1964).
[36] K. J. Vetter, Angew. Chem., Int. Ed. Engl. **1**, 583 (1962).
[37] F. Helfferich, *Ion Exchange* (Dover, New York, 1995), p. 253.
[38] *CRC Handbook of Chemistry and Physics*, 60th ed., edited by R. C. Weast and M. J. Astle (CRC, Boca Raton, FL, 1981), p. D-156.
[39] H. Kanazawa, K. S. Song, T. Sakai, Y. Nakamura, H. Umezawa, M. Tachiki, and H. Kawarada, Diamond Relat. Mater. **12**, 618 (2003).